Received: 18 December 2021 | Accepted: 7 May 2022

DOI: 10.1111/ivb.12379

ORIGINAL ARTICLE

Invertebrate Biology WILEY

A new species of deep-sea torquaratorid enteropneust (Hemichordata): A sequential hermaphrodite with exceptionally wide lips

Nicholas D. Holland | Avery S. Hiley | Greg W. Rouse

Marine Biology Research Division, Scripps Institution of Oceanography, University of California, San Diego, La Jolla, California, USA

Correspondence
Nicholas D. Holland, Marine Biology Research Division, Scripps Institution of Oceanography, University of California, San Diego, La Jolla, CA, USA.
Email: nholland@ucsd.edu

Funding information
David and Lucile Packard Foundation; Schmidt Ocean Institute

Abstract

Specimens of a new species of torquaratorid acorn worm (Hemichordata, Enteropneusta) were video recorded and subsequently collected at abyssal depths in the eastern North Pacific at sites ranging from Oregon to northern Mexico. These worms are described here as *Yoda demiankoopi* n. sp. by molecular and morphological methods. The new species differs from its only described congener, *Yoda purpurata*, in three ways. First, the lips are extremely wide and indented by a deep ciliary groove for ingesting substrate and conveying it to the mouth. Second, a connective tissue bulge of unknown significance runs mid-dorsally along the hepatic and posthepatic regions of the intestine. Third, the posthepatic intestine is strikingly sinuous and packed with gut contents presumably undergoing digestion for extended periods between infrequent defecations. *Yoda demiankoopi* n. sp. is hermaphroditic, a character so far known only for the genus *Yoda* in the entire class Enteropneusta. The gonads of each adult worm comprise hundreds of ovaries (each containing a single oocyte) and hundreds of testes located just beneath the dorsal epidermis of the anterior trunk and associated genital wings. In any given animal, at any given time, gametes of only one sex or the other become fully mature. Thus, the worm is a sequential hermaphrodite, alternately spawning purely as a female or purely as a male.

KEYWORDS
deep-sea, Enteropneusta, Hemichordata, hermaphroditism, Torquaratoridae

1 | INTRODUCTION

Until 2005, acorn worms (class Enteropneusta, phylum Hemichordata) were divided into three families: namely, Spengelidae Willey 1899; Ptychoderidae Spengel 1893; and Harrimaniidae Spengel 1901. At that point, a fourth family, Torquaratoridae Holland et al. 2005, was added to accommodate a clade of deep-sea epibenthic acorn worms, many (and perhaps all) of which periodically ascend above the bottom and drift demersally to new foraging sites. This advance was made possible by the development of remotely operated vehicles (ROVs) capable of video-recording an animal at depth and then bringing the same specimen to the surface for molecular and anatomical studies.

To date, several torquaratorid enteropneusts have been described as new genera and species (Ezhova et al., 2022; Holland et al., 2005,

2009, 2012; Jabr et al., 2018; Osborn et al., 2012, 2013; Priede et al., 2012). In addition to formally named species, others have been collected but still await description. The present study is concerned with one of these undescribed worms—one noteworthy for having extremely wide lips that are indented ventrally by a deep ciliary groove for picking up particulate matter from the substrate and conveying it to the mouth. In previous studies, this worm has informally been referred to as "extrawide–lipped species" (Holland et al., 2009) and as "genus B, species 1" (Osborn et al., 2012). Here, we describe this worm based on molecular analysis and morphology as *Yoda demiankoopi* n. sp. Special attention is given to its unusual reproductive biology.

2 | METHODS

2.1 | Collection and preservation of specimens

The present study is based on worms collected from abyssal depths during three ROV-equipped expeditions. Table 1 is an overview of cruise identification, sampling date, geographic location, collection depth, and museum identification number for each specimen. The bulk of the new information derives from specimens obtained in July 2021, during dives 444 and 445 of the *ROV SuBastian* tended by the research vessel *Falkor* of the Schmidt Ocean Institute. The collection sites (Figure 1, diamond and star) were about 250 km off the Pacific coast of northern Mexico at depths between 1573 and 2476 m. The worms were living exposed on the substrate on the slopes of the Patton Escarpment and the Little Joe Seamount. Each was video recorded for a few minutes (body length was measured by a 10-cm laser scale projected onto the substrate) and then collected by the ROV's slurp system. After the worms reached the deck, a small sample of tissue from each was preserved in 95% ethanol for molecular analysis. Then, the rest of the body was fixed for histological study and conservation in the Scripps Institution of Oceanography Benthic Invertebrate Collection (SIO-BIC). Fixation was in Bouin's fluid (Humason, 1962) for 1 week before storage in 50% ethanol.

Observations were made on three additional worms that had been collected on August 11, 2010, on Dive 176 of the ROV *Doc Ricketts* tended by the research vessel *Western Flyer* of the Monterey Bay Aquarium Research Institute (MBARI). The collection site (Figure 1,

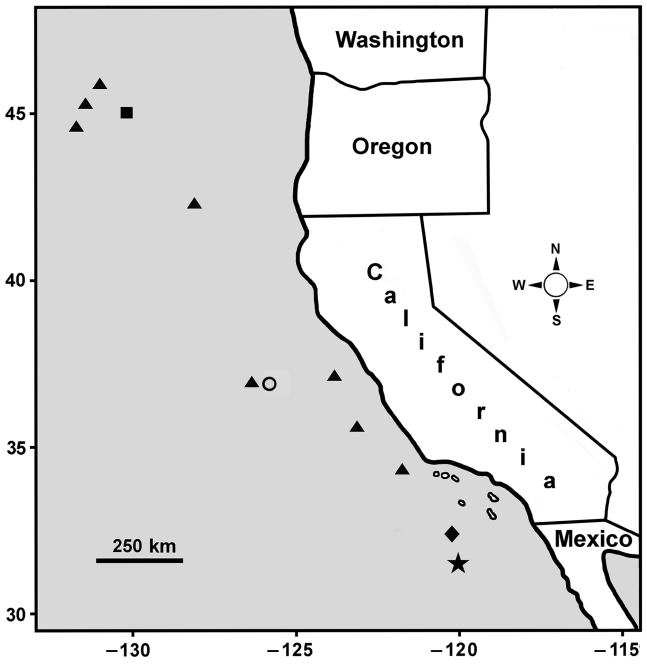

FIGURE 1 *Yoda demiankoopi* n. sp. distribution. The present investigation is based on worms collected at abyssal depths as follows: two specimens from the Patton Escarpment (diamond), two from Little Joe Seamount (star), three from the Taney Seamounts (circle), and two from the Juan de Fuca Ridge (square). In addition, the triangles indicate where specimens were video recorded but not subsequently collected (details in Osborn et al., 2012). Latitude and longitude in degrees are shown on each axis.

TABLE 1 Specimens of *Yoda demiankoopi* n. sp. used in the present study

Catalog number	Designation	Sample date	General Pacific locality	Longitude, latitude	Depth
SIO-BIC H51	Holotype	Jul 30, 2021	Off Mexico	31.900, −120.037	2363 m
SIO-BIC H48	Paratype 1	Jul 29, 2021	Off Mexico	32.403, −120.142	1573 m
SIO-BIC H49	Paratype 2	Jul 29, 2021	Off Mexico	32.402, −120.144	1635 m
SIO-BIC H50*	none	Jul 30, 2021	Off Mexico	31.900, −120.035	2476 m
SIO-BIC H17	Paratype 3**	Aug 11, 2010	Off California	36.850, −125.550	3034 m
SIO-BIC H16	Paratype 4**	Aug 11, 2010	Off California	36.850, −125.550	3034 m
SIO-BIC H15	Paratype 5**	Aug 11, 2010	Off California	36.850, −125.550	3034 m
SIO-BIC H11	none	Aug 13, 2005	Off Oregon	45.147, −130.141	2438 m
SIO-BIC H12	none	Aug 13, 2005	Off Oregon	45.147, −130.141	2438 m

Note: The holotype and all paratypes were histologically sectioned at least in part to assess reproductive state reported in Figure 8. All specimens were sequenced at least for *16S* rRNA for this study or previously (see Table 2). Specimens under each of these catalog numbers include unsectioned fixed tissues and/or serial histological sections.

*Sample used for molecular study only, in ethanol in SIO-BIC, −80°C freezer.

**Gonads only.

circle) was at the Taney Seamounts at a depth of 3034 m. Osborn et al. (2012) used the small ethanol-fixed region of each worm in a molecular phylogenetic analysis but provided no information on their anatomy beyond noting the wide lips; that study designated the worms as "Genus B, sp. 1 (Extra wide-lipped)." The present histological description of the major, formalin-fixed part of each animal was limited to the gonads.

Finally, two worms from 2438 m depth at about 500 km off the Oregon coast (Figure 1, square) were used only in the molecular phylogenetic analysis. They had been collected on August 13, 2005, on Dive 879 of the MBARI ROV *Tiburon* tended by the research vessel *Western Flyer* on the Juan de Fuca Ridge. DNA from these worms had been previously analyzed in Holland et al. (2009), who referred to them as "extrawide-lipped enteropneusts."

2.2 | Molecular phylogenetic analysis

DNA was extracted from the 95% ethanol-fixed tissue samples of the four most recently collected specimens. A Zymo Research DNA-Tissue Miniprep kit was used following the manufacturer's protocol. To place these samples into phylogenetic context with the known torquaratorid sequences available on GenBank, DNA sequences for mitochondrial *16S* rRNA (*16S*) and nuclear *18S* rRNA (*18S*) were generated via Sanger sequencing. Partial *16S* was amplified with primers 16SarL and 16SbrH (Palumbi, 1996), and *18S* was amplified in three overlapping fragments using the following primer pairs: 18S-1F, 18S-5R; 18S-3F, 18S-bi; and 18S-a2.0, 18S-9R (Giribet et al., 1996; Whiting et al., 1997). Polymerase chain reaction (PCR) amplification was carried out with 12.5 μl Apex 2.0× Taq Red DNA Polymerase Master Mix (Genesee Scientific), 1 μl each of the appropriate forward and reverse primers (10 μM), 8.5 μl of ddH_2O, and 2 μl of eluted DNA. DNA sequencing was performed in a thermal cycler (Eppendorf) with the following temperature profiles. Partial *16S* sequences were amplified with the reaction protocol: 180 s at 95°C; followed by 35 cycles of 40 s at 95°C, 40 s at 50°C, and 50 s at 72°C; followed by 300 s at 72°C. Partial *18S* sequences were amplified with two different protocols. 1F/5R and a2.0/9R sequences were amplified with the reaction protocol: 180 s at 95°C; followed by 40 cycles of 30 s at 95°C, 30 s at 50°C, and 90 s at 72°C; followed by 480 s at 72°C. 3F/bi sequences were amplified with the protocol: 180 s at 95°C; followed by 40 cycles of 30 s at 95°C, 30 s at 52°C, and 90 s at 72°C; followed by 480 s at 72°C. PCR products were purified using ExoSAP-IT (USB Affimatrix, Ohio, USA) with the manufacturer's protocol. Sanger sequencing was performed by Eurofins Genomics (Louisville, KY). Consensus sequences were assembled using the De Novo Assembly option on Geneious v.11.0.5 (Kearse et al., 2012) under default settings.

New sequences from the present study were added to data for the same gene regions for other members of Torquaratoridae from previous studies (Cannon et al., 2009; Halanych et al., 2013; Holland et al., 2009; Osborn et al., 2012, 2013). All sequences used are listed in Table 2. One specimen (H89.3R) considered a torquaratorid in fig. 2 of Halanych et al. (2013) was excluded because it was later found not to be a member of this clade by Cannon et al. (2013). Two members of Ptychoderidae were included as outgroups: namely, *Glossobalanus marginatus* MEEK 1922 and *Ptychodera bahamensis* SPENGEL 1893. Sequences were aligned with MAFFT 7 using the G-INS-I setting (Katoh & Standley, 2013). A maximum likelihood (ML) analysis was conducted with RAxML-NG (Kozlov et al., 2019) using RAxML GUI v.2.0.6 (Edler et al., 2021) with 100 random trees. Sequences were concatenated and partitioned by gene, and optimal models were chosen using ModelTest-NG v.0.1.7 (Darriba et al., 2020). Models chosen were TIM2+I+G for *16S* and TN93+I for *18S*. Node support was assessed thorough bootstrapping (with 1000 pseudoreplicates). A Templeton, Crandall and Sing (TCS) haplotype network for the new species of *Yoda* was generated from the nine available *16S* sequences via PopART v.1.7 (Leigh & Bryant, 2015).

For the mitogenomic analysis, the DNA extracted from the SIO-BIC H50 specimen of *Yoda demiankoopi* n. sp. was sequenced on the Illumina Novaseq6000 150-bp platform (Illumina, San Diego, CA) following library preparation by Novogene (en.novogene.com/). The raw genome skimming data set has been deposited in the National Center for Biotechnology Information (NCBI) sequence read archive (SRA) with BioProject accession number PRJNA788979 and BioSample accession number SAMN24044586. Sequence reads were trimmed (leading and trailing low quality or N bases below quality 3 were removed; reads were scanned with a 4-base wide sliding window and cut when the average quality per base dropped below 15; and reads under 36 bp long were dropped) and cleaned of adapters using Trimmomatic v. 0.39 (Bolger et al., 2014). A single mitochondrial genome with an average coverage of 32.8482x was assembled from 6,437,822 paired-end reads using MitoFinder v. 1.4 (Allio et al., 2020). Complete records for all RefSeq Enteropneusta mitogenomes publicly available on NCBI were extracted in GenBank format and used as the reference file for MitoFinder (Allio et al., 2020). The assembly was annotated using the integrated MitoFinder pipeline with MEGAHIT v. 1.2.9 (Li et al., 2016) and ARWEN v. 1.2 (Laslett & Canbäck, 2008), as well as the MITOS web server (Bernt et al., 2013). The annotated assembly was modified using Geneious v. 11.1.5 (Kearse et al., 2012). The mitochondrial genome contains 17,004 bp, and the assembly had a Guanosine-Cytosine (GC) content of 40.37% and included 13 protein-coding genes (PCGs), 2 ribosomal RNA (rRNA) genes, and 22 transfer RNA (tRNA) genes.

The newly assembled and annotated mitogenome for *Yoda demiankoopi* n. sp. (SIO-BIC H50) has been deposited in GenBank under the accession number OL693683. The 15 mitochondrial genes (2 rRNAs and 13 PCGs) sourced from the finalized mitogenome of *Yoda demiankoopi* n. sp. and the terminals used by Li et al. (2019), fig. 3) were extracted in Geneious v. 11.1.5 (Kearse et al., 2012). Nucleotide (NT) alignments of the two rRNAs were performed in Mesquite v. 3.61 for each gene using the MUSCLE algorithm (Edgar, 2004) with default settings. The 13 PCGs were translated into amino acids (AAs) with all final stop codons removed, and resulting AA sequences for each PCG were aligned in Mesquite v. 3.61, also using MUSCLE with default settings.

TABLE 2 GenBank accession numbers for sequences used in the phylogenetic analyses shown in Figure 2A

Taxon	Sources	*16S* accession numbers	*18S* accession numbers
Torquaratoridae			
Allapasus aurantiacus	Osborn et al. (2012)	JN886748, JN886750	JN886765, JN886767
Allapasus isidis	Osborn et al. (2012)	JN886749	JN886766
Coleodesmium karaensis	Osborn et al. (2013)	KC907711	KC907710
H78 = *Coleodesmium karaensis*	Cannon et al. (2013)	KF683553*	KF683565
Quatuoralisia malakhovi	Ezhova et al. (2022)	MT773355-59	
Tergivelum baldwinae	Holland et al. (2009); Osborn et al. (2012)	EU520494-97	EU520506, EU520508-09, JN886772**
Tergivelum cinnabarinum	Osborn et al. (2012)	JN886752-54	JN886769-71
Yoda purpurata	Osborn et al. (2012)	JN886740-42	JN886757-59
Yoda demiankoopi n. sp. (Oregon)	Holland et al. (2009); Osborn et al. (2012)	EU520500-01	EU520513, JN886760***
Yoda demiankoopi n. sp. (California)	Osborn et al. (2012)	JN886744-46	JN886761-63
Yoda demiankoopi n. sp. (off Mexico)	**This study**	**OL693683, OL889883-85**	**OL889880-81**
IFREMER *Yoda*	Cannon et al. (2009)	EU728431	EU728438
Narrow-lipped/Genus C	Holland et al. (2009); Osborn et al. (2012)	EU520498-99, JN886751	EU520510-11, JN886768
H90 Antarctica	Halanych et al. (2013); Cannon et al. (2013)	KF683552	KF683564
Outgroups			
Glossobalanus marginatus	Cannon et al. (2013)	KF683559	KF683566
Ptychodera bahamensis	Worsaae et al. (2012)	JX855285	JF900485

Note: New sequences are in bold.
*Recorded as Torquaratoridae H78.1 from Antarctica on GenBank, but as H78.1 from Iceland in Cannon et al. (2013, 2014).
**JN886772 (Osborn et al., 2012) was used instead of EU520507 (Holland et al., 2009) as it was a more complete sequence from the same specimen.
***JN886760 (Osborn et al., 2012) was used instead of EU520512 (Holland et al., 2009) as it was a more complete sequence from the same specimen.

An ML analysis with 100 random starting trees was performed using raxmlGUI v. 2.0.6, and node support was assessed via the thorough bootstrapping option, with 1000 pseudoreplicates. Data were partitioned by gene, with best-fit models for these partitions selected using ModelTest-NG v. 0.1.7. ATP6, COX1, COX2, COX3, CYTB, ND1, ND2, ND3, ND4, and ND4L were assigned the MTZOA model; ATP8 and ND5 were assigned the MTREV model; ND6 was assigned the JTT model; and *12S* and *16S* rRNA genes were assigned the GTR+I+G model. The tree was rooted with the Echinodermata terminals from Li et al. (2019).

2.3 | Histology and histochemistry

For histological examination, tissues were embedded in paraplast and prepared as serial sections cut 12 μm thick. Staining was in hematoxylin for nuclei (Gill et al., 1974), in Ponceau for protein (previously unpublished procedure: 1 min in 0.1% Ponceau S in 1% aqueous acetic acid) or in the following mucus stains: azure A (Casselman, 1959), alcian blue (Humason, 1962), or periodic acid–Schiff (PAS) (Humason, 1962). In the present paper, most of the histological illustrations show sectioned tissues of the holotype; exceptions are noted in the figure legends.

2.4 | Quantification of gonadal development

All specimens examined were hermaphrodites, each with numerous ovaries and numerous testes. The reproductive state was assessed quantitatively in the holotype and in Paratypes 1–4 (Paratype 5, although too poorly fixed to assess reproductive state quantitatively, resembled Paratype 4 qualitatively). For the oocytes (each corresponding to a single ovary), size–frequency polygons were constructed by the method of Pearse (1965): In serial histological sections of each worm, the diameters of the first 50 oocytes encountered in nucleolar section were measured. For elliptical oocytes, the diameter was calculated as the average of the long and short axes. The oocyte size range from 0 to 480 μm was divided into 12 classes at 40-μm intervals, and the percentage of oocytes in each class was plotted. In addition, for each animal, 50 testes were measured in their maximum diameter (determined by scanning serial sections), and the mean diameter was calculated ± one standard deviation.

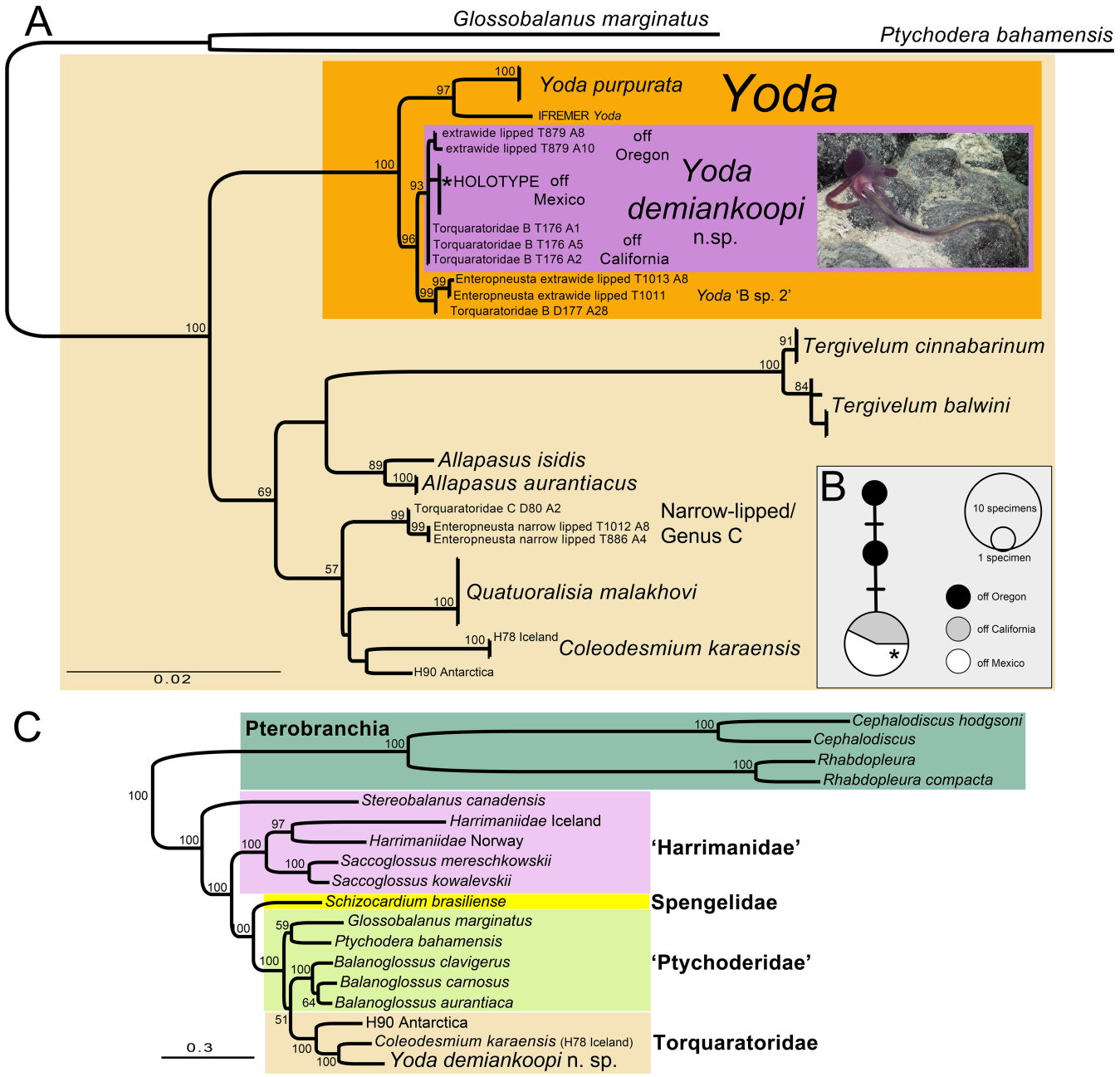

FIGURE 2 (A) Maximum likelihood (ML) phylogenetic tree generated for Torquaratoridae from the concatenation of mitochondrial *16S* rRNA and nuclear *18S* rRNA genes shown in Table 2. Small text names for Torquaratoridae terminals are those listed on GenBank. Numbers on nodes represent ML bootstrap values. (B) *Yoda demiankoopi* n. sp. *16S* rRNA haplotype network. Specimens were collected from three general regions: off Oregon, off California, and off Mexico (Table 1). The haplotype and locality of the holotype are indicated by the asterisk. (C) ML tree for Hemichordata generated from the concatenation of 13 protein-coding genes (as amino acids) and two ribosomal genes (as DNA). Numbers on nodes represent ML bootstrap values. The echinoderm outgroups have been omitted. Apart from the newly generated mitogenome of *Yoda demiankoopi* n. sp. (GenBank accession number OL693683), the terminals shown here were sourced from Li et al. (2019). The live image of *Yoda demiankoopi* n. sp. (Paratype SIO-BIC H50) courtesy of the Schmidt Ocean Institute. Scale bars show expected numbers of substitutions per site.

3 | RESULTS AND DISCUSSION

3.1 | Phylogenetic analyses

The ML phylogenetic analysis of the concatenated *18S* and *16S* sequence data (Figure 2A) recovered a similar topology to that found in the most recent analysis of Torquaratoridae (Cannon et al., 2013; Osborn et al., 2013) and to the *16S*-only analysis of Ezhova et al. (2022). The differences in topology reflect the poor support for those nodes in previous studies and here. The well-supported clade that is here delineated as *Yoda* had previously been referred to as containing two undescribed genera, Genus A and Genus B (Osborn et al., 2012). Following the description of *Yoda purpurata* for Genus A, the undescribed Genus B was maintained with two undescribed species (Osborn et al., 2013; Priede et al., 2012). We see no reason to erect a new genus for Genus B, and so *Yoda* now also includes the new species being formally described below as *Yoda demiankoopi* n. sp., as well as two yet to be described species (Figure 2A). *Yoda demiankoopi* n. sp. is the well-supported sister group to one of these new species (*Yoda* "B sp.2"), and this pair is the sister group to *Yoda purpurata* and the undescribed IFREMER *Yoda* (Figure 2A). In addition to the previously available sequences for *Yoda demiankoopi* n. sp., we added data for four more specimens and extended its range south to Mexico from California and Oregon (Figure 1). The *18S* sequences were invariant across all the samples of *Yoda demiankoopi* n. sp. The *16S* haplotype network (Figure 2B) showed that all California and Mexico specimens shared the same haplotype, whereas the two Oregon specimens were one or two bases different.

Yoda, as delineated here, has been consistently recovered as a well-supported clade that is the sister group to all other Torquaratoridae (Figure 2A). The phylogenetic analysis of the 13 PCGs and 2 rRNAs from the whole mitochondrial genomes found *Yoda demiankoopi* n. sp. to be the well-supported sister group to *Coleodesmium karaensis* (Figure 2C). The undescribed taxon "H90 Antarctica" was then recovered as the sistergroup to *Yoda demiankoopi* n. sp. +- *C. karaensis*. This differs markedly from the combined 18S + *16S* result in which H90 Antarctica was the sister group to *C. karaensis*, though with low support (Figure 2A). Unfortunately, H90 Antarctica was evidently not studied morphologically by Halanych et al. (2013) (their fig. 1b might show the specimen, although their text is not clear on this point).

Allowing for the addition of *Yoda demiankoopi* n. sp., the overall topology of Hemichordata shown in Figure 2C is like that found in Li et al. (2019). This indicates that Torquaratoridae is nested inside Ptychoderidae even though the support for the Torquaratoridae + *Balanoglossus* clade was quite low (Figure 2C; Li et al., 2019). Although prior analyses of ribosomal genes had shown Ptychoderidae and Torquaratoridae to be reciprocally monophyletic (Cannon et al., 2013; Osborn et al., 2012, 2013), the paraphyly of Ptychoderidae with respect to Torquaratoridae has been recovered in a previous transcriptomic study (Cannon et al., 2014); however, support for the Torquaratoridae + *Balanoglossus* clade was again low in that analysis. Nevertheless, the much larger data sets now available for mitogenomics and transcriptomics suggest that further data and analysis could support Torquaratoridae as a clade within Ptychoderidae, which would reduce the rank of the former to subfamily.

3.2 | Taxonomy

Phylum Hemichordata Bateson 1885
Class Enteropneusta Gegenbaur 1870
Family Torquaratoridae Holland et al. 2005
Genus *Yoda* Priede et al. 2012

3.2.1 | Diagnosis (emended)

This genus of Torquaratoridae has the collar with a pair of extended lateral lips. These can be either be (1) gradually tapering lateral lips, each three times longer than its anterior–posterior dimension basally; or (2) extremely wide, non-tapered lips. A conical nuchal protuberance projecting dorsally from the anterior dorsal ridge of the collar on either side of the midline may be absent or present. A sinuous posthepatic intestine may be absent or present. Anterior body color can be reddish to brownish purple or translucent white. Hermaphroditism is present.

3.2.2 | Remarks

Part of the generic diagnosis of *Yoda* in Priede et al. (2012) was based on the presence of neck ridges and nuchal protuberances, which are lacking in *Yoda demiankoopi* n. sp., and the diagnosis is thus emended here to allow for its absence. Also, the condition of the lips for the genus can be in two forms, gradually tapering in *Yoda purpurata* and extremely wide, non-tapering in *Yoda demiankoopi* n. sp. and in the presently undescribed *Yoda* "B sp. 2" (see fig. 1h in Osborn et al., 2012). The sinuous posthepatic intestine found in *Yoda demiankoopi* n. sp. and *Yoda* "B sp. 2" is lacking in the type species *Yoda purpurata*. The hermaphroditism found in *Yoda* studied to date is unique across all Enteropneusta.

3.2.3 | *Yoda demiankoopi* n. sp. Holland, Hiley & Rouse 2022

http://zoobank.org/urn:lsid:zoobank.org:act:D6F2A5B9-BC73-4F44-90ED-70548656B5F2

Type material

Holotype. SIO-BIC H51 from Little Joe Seamount (31.900, −120.037) at 2363 m on rocky slope. ROV *SuBastian* Dive 445 on July 30, 2021, collected by G. Rouse and N. Mongiardino Koch. Specimen was fixed in Bouin solution with a subsample into ethanol for DNA sequencing. The specimen was subsequently histologically sectioned. The *16S*

rRNA sequence for the holotype has the GenBank Accession number OL889885.

Paratypes. See Table 1.

Diagnosis. This species of *Yoda* has the proboscis, collar, and genital wings with a deep brownish purple color, which continues with fading intensity along the posterior body. Neck ridges and nuchal protuberances are absent. The collar has extremely wide, non-tapered lips. The posthepatic intestine, in the last third of the body, shows a marked sinuosity. Adults are simultaneous hermaphrodites.

Remarks. *Yoda demiankoopi* n. sp. can clearly be distinguished from *Yoda purpurata* because the former has (1) extremely wide, non-tapered lips; (2) a mid-dorsal connective tissue bulge running along the hepatic and posthepatic regions of the intestine; and (3) a sinuous posthepatic intestine. However, the sister group to *Yoda demiankoopi* n. sp., shown on Figure 2A as *Yoda* "B sp. 2," also does have extremely wide, non-tapered lips and the sinuosity of the posthepatic intestine (see fig. 1h in Osborn et al., 2013). These two can be distinguished visually in life because *Yoda* "B sp. 2" lacks the deep brownish purple color anteriorly that characterizes *Yoda demiankoopi* n. sp. *Yoda demiankoopi* n. sp., and *Yoda* "B sp. 2" do not particularly resemble the Star Wars character named *Yoda*, unlike the type species *Yoda purpurata*, but the close relationship phylogenetically allows us to apply the name *Yoda* more generally. There is no information on the morphology of the sister group to *Yoda purpurata*, shown in Figure 2A as IFREMER *Yoda*.

Etymology of species name. Latin masculine genitive noun *demiankoopi*. The name commemorates Dr. Demian Koop of the University of Sydney, a passionate developmental biologist and exceptional scientist whose very untimely death in 2021 has been keenly felt by his friends and colleagues all over the world.

3.2.4 | Extended description including living appearance, gross anatomy, and behavior

The living lengths of the worms described here were holotype = 32.0 cm; paratype 1 = 14.9 cm; paratype 2 = 19.5 cm; paratype 3 = 30.5 cm; paratype 4 = 27.0 cm; and paratype 5 = 31.3 cm. Figure 3 shows the gross anatomical features, with major body parts labeled. In most of the video recordings, the pharyngeal region of the body was hidden beneath the genital wings, but one favorably oriented animal showed the most posterior pharyngeal gill pores (Figure 4B, arrowhead).

The color of the proboscis, collar, and lips was deep brownish purple under the lights of the ROV (Figure 4A,B) but was recorded more accurately as reddish purple for animals photographed alive immediately after recovery (Figure 4C,D). The delicate genital wings and lateroventral folds were a much lighter purple. All the specimens described

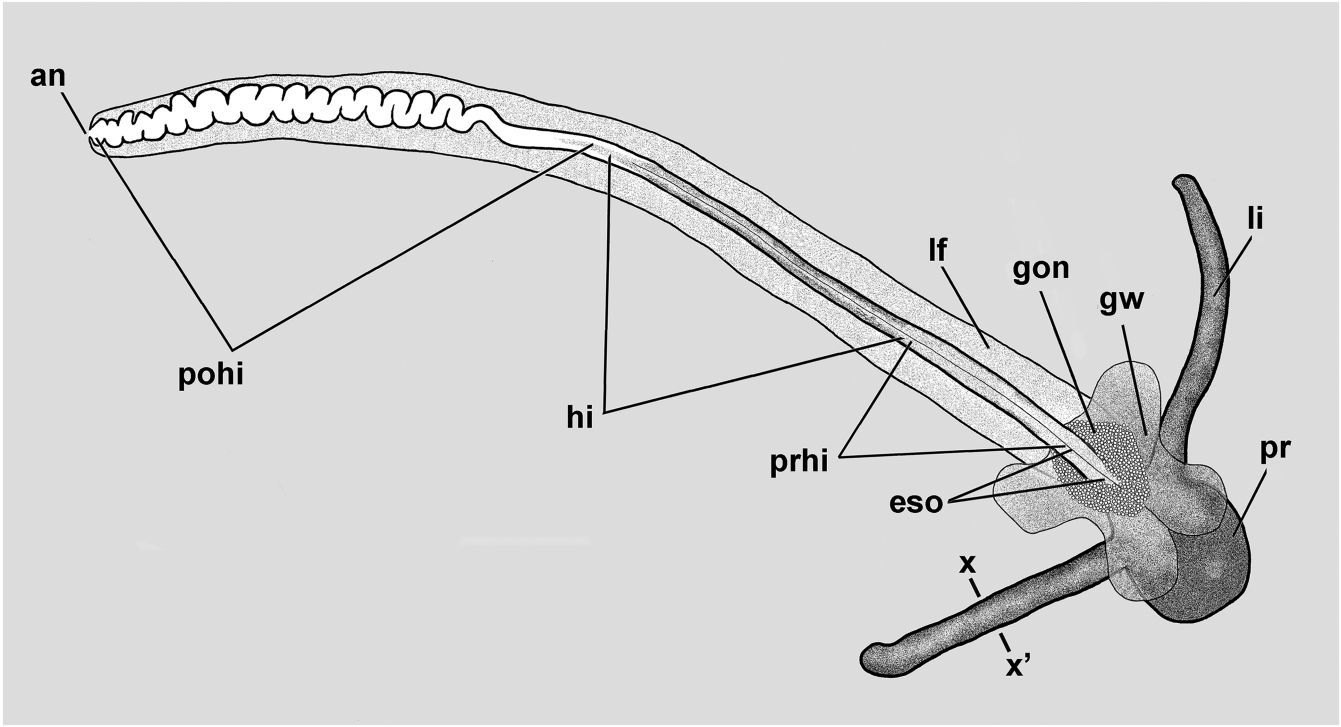

FIGURE 3 *Yoda demiankoopi* n. sp. Drawing from videorecording of living holotype (SIO-BIC H51) and its major body parts. an, anus; eso, esophagus; gon, gonads; gw, genital wing; hi, hepatic intestine; lf, lateroventral fold; li, lip; pohi, posthepatic intestine; pr, proboscis; prhi, prehepatic intestine; x–x′, location of cross section in Figure 5H

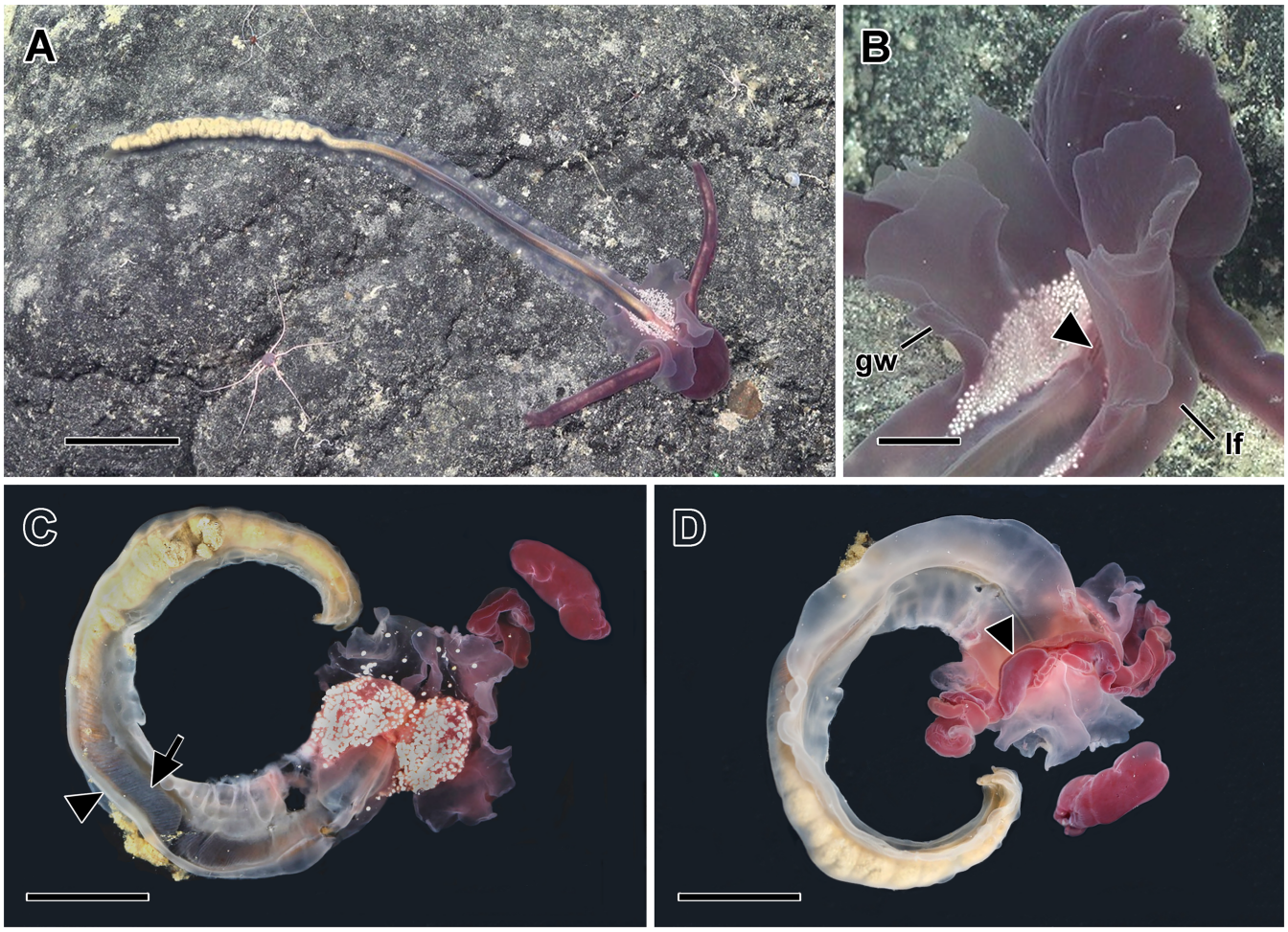

FIGURE 4 *Yoda demiankoopi* n. sp. (A) Living holotype SIO-BIC H51. (B) Specimen SIO-BIC H50, showing lateroventral folds (lf), genital wings (gw), and most posterior gill pores (arrowhead). (C) Dorsal view of holotype soon after reaching the deck; arrow indicates dark hepatic intestine; arrowhead indicates mid-dorsal connective tissue bulge. Broken-off proboscis is at top right. (D) Ventral view of foregoing with ciliary groove (arrowhead) on ventral side of lip. Images 4A and 4B captured by Schmidt Ocean Institute's ROV *SuBastian* on cruise FK210726. Images owned by SOI. Scale bars: A = 5 cm; B = 1 cm; C,D = 2 cm

here were hermaphrodites with a gonadal region comprising numerous testes and numerous ovaries located just beneath the dorsal epidermis of the pharyngeal and esophageal regions and in the genital wings. Gonads of both sexes were, at most, about 500 μm in diameter and were cream colored in living worms (Figure 4A–C). The hepatic intestine was a blackish brown (Figure 4C, arrow) because of an abundance of dark pigment granules in its lining epithelial cells, and the posthepatic intestine appeared yellowish, which was the color of the luminal contents visible through the relatively transparent surrounding tissues.

In the field, the worms were typically seen with the ventral surface closely applied to the very thin layer of soft sediment overlying the hard substratum; the latter consisted of a ferromanganese veneer encrusting the basalt beneath (the detailed geology of Little Joe Seamount is discussed by Hein et al., 2010). The worms crawled very slowly, evidently by the action of cilia on the ventral surface of their lips, lateroventral folds, and main axis of the body (there is little doubt that such cilia were present, although they could not be demonstrated in our histological sections, apparently because of damage to the epidermis caused by swelling mucus when the worms were fixed). When a worm was crawling forward on a relatively flat surface, the lips were well extended, bending only slightly posteriorly. In contrast, when a worm was on a substrate with irregular topography, the lips could be much contorted.

The lips harvested a wide swath of substrate that apparently included a considerable amount of sunken marine snow (Rouse, unpubl. data). The substrate was taken into a deep ciliary groove (described in detail below) running along the entire ventral side of each lip. As seen in the living animal, the lip (Figure 4A, arrowhead) was about 3.5 mm in diameter. Because the lip tissue is semitransparent, the cord of ingested materials in the capacious ciliary groove was visible and, in many places, reached a diameter approaching 2 mm. The contents within the ciliary groove were passed to the mouth to enter the main course of the gut. The ingested matter in the ciliary groove of the lips and in the gut lumen included few hard objects (e.g., mineral grains, sponge spicules, diatom valves,

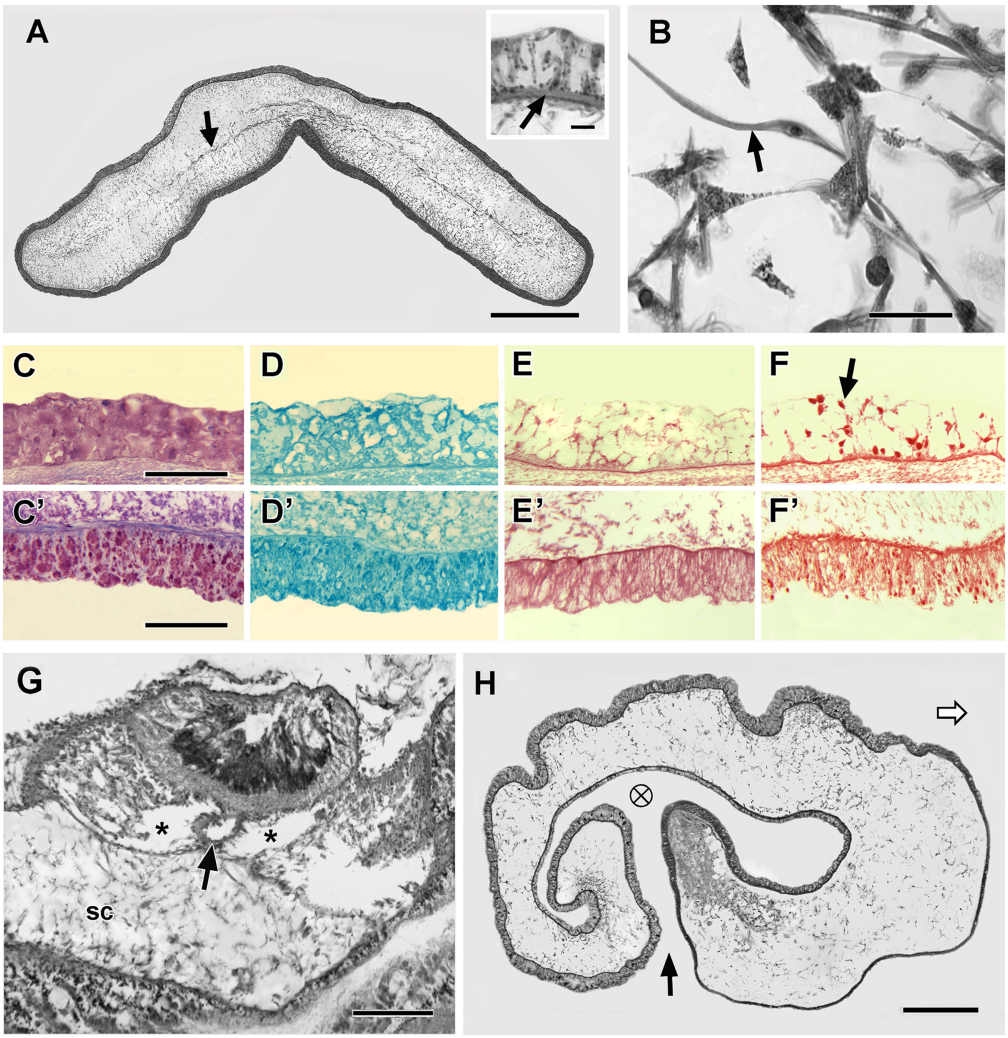

FIGURE 5 *Yoda demiankoopi* n. sp. Holotype SIO-BIC H51 (5A–F,H), paratype SIO-BIC H47 (5G). (A) Cross section near anterior end of the proboscis; arrow indicates a lamina of fibrous connective tissue. Azure A. Inset in A: enlargement of dorsal epidermis showing nuclei and basal nerve fiber layer (arrow). Hematoxylin. (B) Connective tissue of proboscis, comprising connective tissue fibers, smooth muscles (arrow), and free cells. Ponceau. (C–F) Dorsal epidermis of proboscis stained, respectively, with azure A, alcian blue, periodic acid–Schiff (PAS), and Ponceau; arrow in F indicates a local strong reaction for protein. (C′–F′) Ventral epidermis of proboscis stained, respectively, with azure A, alcian blue, PAS, and Ponceau. (G) Cross section of collar nerve cord (top center) overlying dorsal hemal vessel (arrow), perihemal coeloms (asterisks), and stomochord (sc). Hematoxylin. (H) Cross section of lip on right side (through x–x′ in Figure 2). White arrow shows direction of crawling, black arrow indicates opening to ciliary groove, and cross-in-circle engineering symbol indicates substrate in groove is conveyed into page. Azure A and Ponceau. Scale bars: A = 2 mm; Inset A = 50 μm; B = 25 μm; C–F, C′–F′ = 200 μm; G = 250 μm; H = 500 μm

and foraminiferan tests) but instead consisted chiefly of unrecognizable soft material packing the gut lumen; it is not known whether any selectivity was involved in the ingestion of the sediment. Except in exceptional cases (see below), the gut contents were lost from the lip ciliary grooves and gut lumen during histological processing.

Strikingly, in contrast to other torquaratorid species (including *Yoda purpurata*), the video-recorded holotype and paratypes of *Yoda demiankoopi* n. sp. were not seen at the head of a fecal trail. Presumably, the gut contents are retained for long periods and only periodically extruded from the anus during major defecation events.

3.3 | Histological structure

The histological structures will be described here in order from anterior to posterior. The proboscis, as seen in cross section at a relatively anterior level (Figure 5A), was bounded by an epidermis of columnar cells underlain by a basal nerve fiber layer (inset in Figure 5A). The epidermis enclosed a loose interior meshwork of smooth muscles and connective tissue of fine fibrils and scattered free cells (Figure 5B). Some of the connective tissue fibers were organized into a loosely woven horizontal septum (Figure 5A, arrow) of unknown significance.

When the epidermis of the proboscis was studied histochemically, some differences between the ventral and dorsal sides of the body

were apparent. By the criteria of Spicer (1963), the epidermal cells covering the dorsal and ventral sides of the proboscis were rich in acid mucopolysaccharides, both sulfated (violet color indicates gamma metachromatic staining with azure A, shown in Figure 5C,C′) and non-sulfated (staining with alcian blue, shown in Figure 5D,D′). An additional feature, limited to the ventral epidermis, was a moderate PAS reaction for neutral mucus (Figure 5E′). Moreover, staining with Ponceau showed that the ventral epidermal cells were protein rich (Figure 5F′), whereas the cells of the dorsal epidermis were not, except for some oval proteinaceous inclusions (Figure 5F, arrow); the latter were evidently the contents of the widely scattered goblet cells that Benito (1975) previously described in the epidermis of shallow-living enteropneusts. Importantly, the same histochemical differences between the dorsal and ventral epidermis, as illustrated here for the proboscis, were consistently observed throughout the dorsal and ventral epidermis of the more posterior body regions.

Yoda demiankoopi n. sp. was exceptionally easy to damage during collection. Thus, in the holotype and all the paratypes, the proboscis had separated from the rest of the worm (e.g., Figure 4C,D), and structures of the anterior collar and proboscis stalk were distorted or broken. Even so, a collar nerve cord underlain by the dorsal hemal vessel and paired perihemal coeloms could be demonstrated (Figure 5G). Ventral to these structures ran a stomochord, but no trace of a proboscis skeleton was seen. Despite damage to tissues in this region, it could be determined that the anterior end of the collar nerve cord extended as two large nerves (not illustrated here), one on either side of the proboscis stalk, at the base of the epidermis.

In its external features, the collar of *Yoda demiankoopi* n. sp. differed strikingly from that of *Yoda purpurata*. The former includes neither an anterior dorsal ridge with nuchal protuberances nor a posterior dorsal ridge. Moreover, as already mentioned, the lips of *Yoda demiankoopi* n. sp. are strikingly wider than those of *Yoda purpurata*. A cross section through a lip of *Yoda demiankoopi* n. sp. (through x–x′ in Figure 3) showed a deep ciliary groove, mushroom-shaped in profile in the sectioned material (Figure 5H). The opening to the groove (Figure 4D, arrowhead; and Figure 5H, black arrow), which appeared as a relatively narrow slot when viewed running along the ventral side of the lip, is somewhat offset posteriorly. The epidermis anterior to the groove was about 35 μm thick and consisted of protein-rich cells that were presumably heavily ciliated. In contrast, the epidermis posterior to the groove was about 200 μm thick and made up predominantly of mucous cells. Epidermal cilia anterior to the opening evidently sweep substrate into the groove, whereas the epidermis posterior to the opening adds mucus that binds the entering particulate material, insuring its capture and transport to the mouth.

Cross sections of the pharynx (Figure 6A) showed a dorsoventrally compressed lumen that curled dorsally on either side. The epithelium lining of this gut region was smooth in contour. Just beneath the dorsal epidermis of the pharynx (and the following esophagus) were gonads that will be covered in detail in Section 3.4. Mid-dorsally in the pharynx, a short mesentery connected the gut lining with the dorsal nerve cord in the epidermis (Figure 6A, single arrow). Similarly, a mid-ventral mesentery connected the gut lining with the ventral nerve cord (Figure 6A, arrowhead). These midline nerves (and their underlying hemal vessels) continued along the more posterior trunk regions. The basal side of the ventral epidermis in the pharyngeal region was associated with relatively inconspicuous muscle cells that were longitudinally oriented (inset in Figure 6A, arrowhead), thus contrasting with the even more sparse muscles randomly oriented elsewhere in the connective tissue. This longitudinal musculature was associated with the ventral epidermis along the entire ventral side of the main body axis and lateroventral folds.

The branchial apparatus was located along the dorsomedial portion of the pharynx and consisted of alternating primary and secondary gill bars (Figure 6B). The slots between the gill bars opened dorsally into atria that, in turn, emptied to the exterior at the gill pores (Figure 6A,C). The total number of gill bars and pores in *Yoda demiankoopi* n. sp. could not be determined because of damage toward the anterior end of the pharynx in all specimens available for study.

The epithelium lining the esophagus and the three intestinal regions—in contrast to the relatively smooth lining of the pharynx—appeared as alternating ridges and troughs (Figure 7A–E). This pattern did not result from alternating thick and thin areas of epithelium, but instead reflected the topography of the underlying connective tissue. The ridges and troughs were organized as a set of parallel spirals of the fibrous connective tissue running along the anterior–posterior axis of the digestive tract.

In the prehepatic intestine (Figure 7B), the lining epithelium was very thin, thus contrasting with its thicker counterpart lining the other gut regions. Another peculiarity of the prehepatic intestine was the much greater abundance of sulfated mucopolysaccharides in the connective tissue ridges (inset in Figure 7B) in comparison with the connective tissue ridges in the other gut regions (insets in Figure 7C,E). It is unclear what function is served by these mucopolysaccharide-rich regions in the subepithelial connective tissue of the prehepatic intestine; perhaps they provide some mechanical support for the ridged lining of the organ. One might also be tempted to propose that mucus abundantly produced and mixed with the food during ingestion is partially salvaged by uptake through the epithelium lining the prehepatic intestine. However, no matter how useful such salvage would be to a ciliary-mucoid feeder, there appears to be no precedent for such transepithelial transport of mucopolysaccharides in other biological systems.

The next part of the gut studied was the hepatic intestine. Based on cell fine structure, this region is thought to be involved in extracellular and intracellular digestion in acorn worms generally (Benito et al., 1993), although functional studies are so far lacking. In *Yoda demiankoopi* n. sp., the hepatic (as well as the posthepatic) intestine was characterized by a prominent mid-dorsal bulge of connective tissue (Figures 4C–7C) of unknown significance. This does not appear to be an artifact because animals *in situ* showed the bulge as well (Figures 2 and 4A). The dorsal wall of the hepatic intestine lacked the sacculations characterizing this gut region in some enteropneusts. However, as is common in enteropneusts, many epithelial cells lining

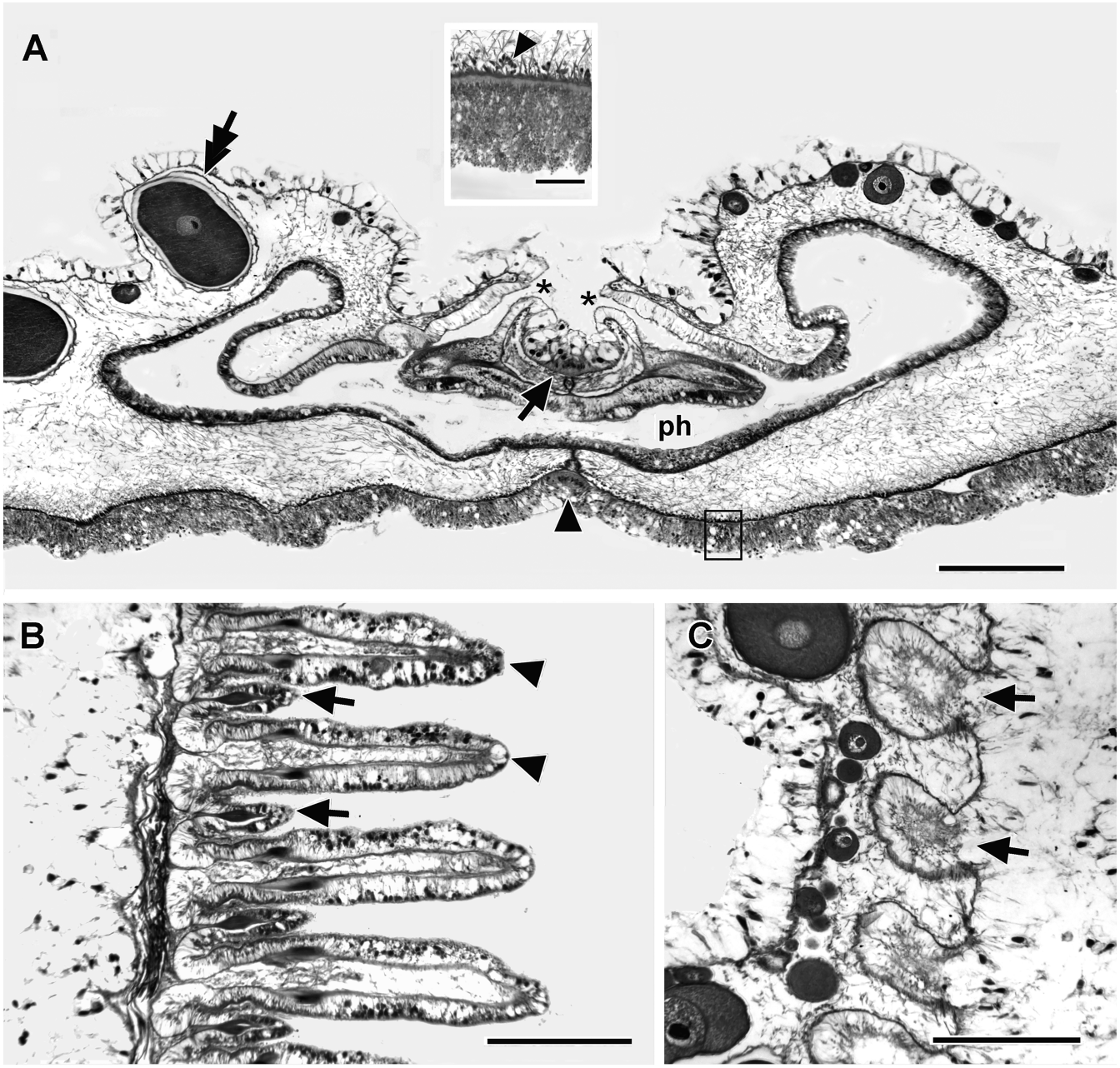

FIGURE 6 *Yoda demiankoopi* n. sp. Holotype SIO-BIC H51 (6A), paratype SIO-BIC H46 (6B, C). (A) Cross section of pharynx (ph), gill pores (asterisks), dorsal nerve cord (single arrow), ventral nerve cord (arrowhead), and ovary (tandem arrow) with single large oocyte surrounded by jelly layer. Ponceau. Inset in A: enlargement of boxed area showing inconspicuous longitudinal muscle fibers (arrowhead). (B) Frontal section through branchial apparatus; arrows indicate primary gill bars (septa), and arrowheads indicate secondary gill bars (tongue bars). (C) Frontal section through gill pores (arrows). Scale bars: A = 500 μm; Inset A = 100 μm; B,C = 250 μm

the hepatic intestine were filled with fine dark pigment granules (Figure 7D).

The most posterior division of the gut, the posthepatic intestine, had the mid-dorsal connective tissue bulge already mentioned (Figures 2, 4A,C, and 7E), but by far the most conspicuous feature of this gut region was its sinuous course (Figure 3). This topography permits the retention of a large volume of gut contents with only a relatively modest increase in body length. A similar tendency of abyssal detritivores to have enlarged hindgut capacity has also been observed in some deposit-feeding mollusks (Steiner, 1994), and it is thought that this gut region is an important site of digestion and absorption of nutrient-poor abyssal sediments. In *Yoda demiankoopi* n. sp., no fecal trails were detected in nature posterior to the living holotype or the paratypes. Thus, the contents of the posthepatic intestine are evidently retained for long periods of time between major episodes of defecation. The prolonged retention of voluminous gut contents is

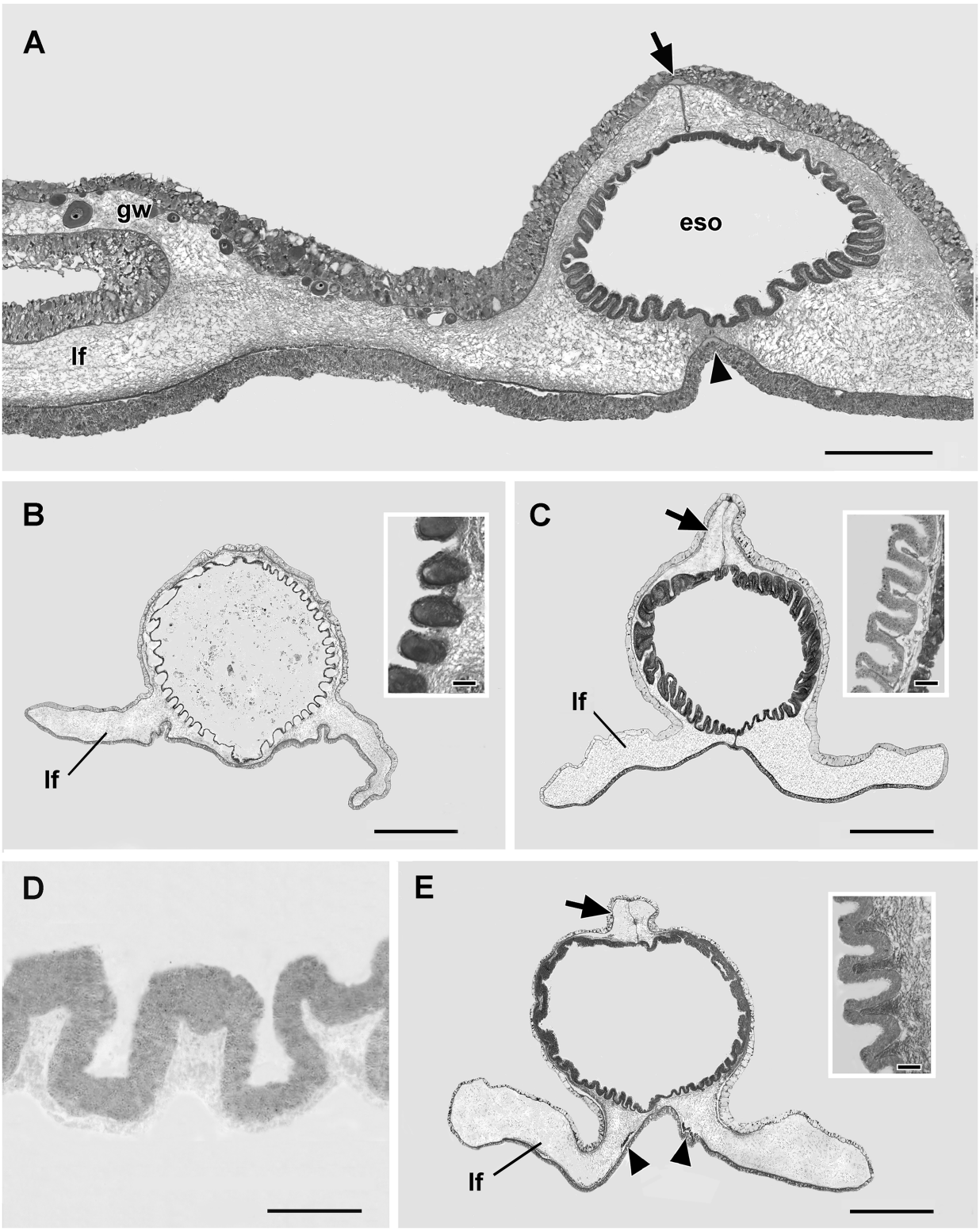

FIGURE 7 *Yoda demiankoopi* n. sp. Holotype SIO-BIC H51. (A) Cross section through esophagus, dorsal nerve cord (arrow), ventral nerve cord (arrowhead), genital wing, and lateroventral fold. Azure A. (B) Cross section through prehepatic intestine (with gut contents) and lateroventral folds. Ponceau. Inset in B: gut wall stained with azure A. (C) Cross section through hepatic intestine (gut contents lost during dissection) with lateroventral fold and mid-dorsal connective tissue bulge (arrow). Inset in C: gut wall stained with azure A. (D) Unstained hepatic intestine lined with epithelial cells containing dark pigment granules. (E) Cross section through posthepatic intestine (gut contents lost during dissection) with lateroventral fold, mid-dorsal connective tissue bulge (arrow), and two conspicuous muscle bundles (arrowheads). Inset in E: gut wall stained with azure A. Scale bars: A = 1 mm; B = 2 mm; Inset B = 200 μm; C = 2 mm; Inset C = 200 μm; D = 500 μm; E = 2 mm; Inset E = 200 μm. eso, esophagus; gw, genital wing; lf, lateroventral folds

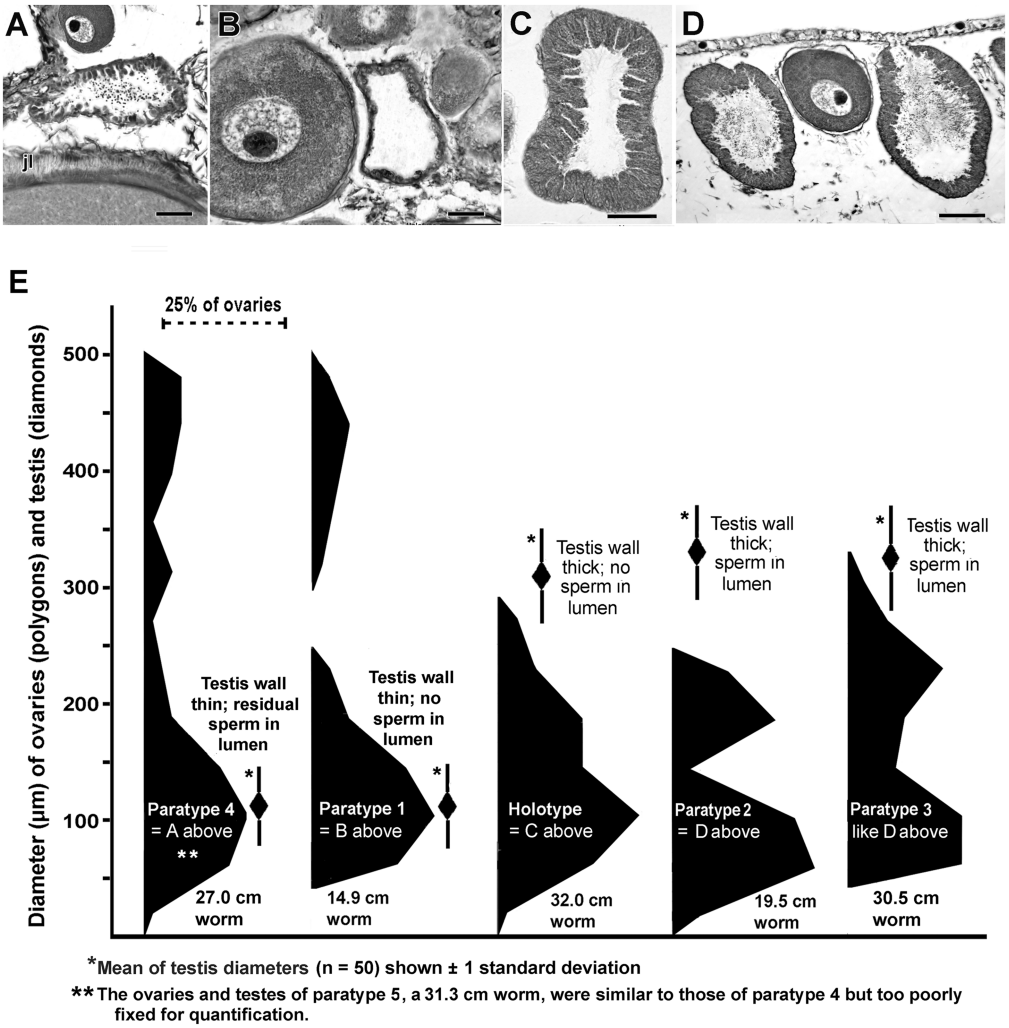

FIGURE 8 *Yoda demiankoopi* n. sp. Paratype SIO-BIC H16 (8A), paratype SIO-BIC H46 (8B, holotype SIO-BIC H51 (8C), paratype SIO-BIC H47 (8D) (A) Gonads of paratype 4. From top: ovary with small oocyte, testis with thin germinal epithelium and residual sperm in lumen, and periphery of ovary with large oocyte showing jelly layer (jl). Hematoxylin stained (as are B–D). (B) Gonads of paratype 1. From left: ovary with medium-sized oocyte and testis with thin germinal epithelium surrounding empty lumen. (C) Testis of holotype with thick germinal epithelium and no sperm in lumen. (D) Gonads of paratype 2. Ovary with medium-sized oocyte flanked by two testes, each with a thick germinal epithelium and sperm in lumen. (E) Size–frequency polygons for oocytes in holotype and paratypes; each polygon is based on diameters of 50 oocytes (=ovaries). Also shown for each specimen is the mean diameter of the testes ± one standard deviation ($n = 50$). Scale bars: A,B = 50 µm; C,D = 100 µm

interesting in the light of new ideas about the role of bacterial communities in the guts of deep-sea deposit-feeding animals (Romero-Romero et al., 2021). It is possible that individuals of *Yoda demiankoopi* n. sp. might assimilate molecules released when gut microbes digest refractory organic material, or the worm might directly harvest the bacteria themselves as a source of nutrition, or both.

The posthepatic intestine also differed from more anterior gut regions in having a prominent bundle of longitudinal muscles running just beneath the epidermis on either side of the ventral midline (Figure 7E). These bundles seem to be simply an exaggeration of the inconspicuous longitudinal muscles associated with the ventral surface of the trunk in general (Figure 6A, inset). The enlarged muscles might slowly churn the hindgut to facilitate digestion and nutrient absorption. In addition, they might contract strongly to help expel the gut contents during the presumed episodes of sudden defecation.

3.4 | Gonads and reproductive biology

As already mentioned, all specimens of *Yoda demiankoopi* n. sp. described here were hermaphrodites, each having a gonadal region comprising hundreds of testes and hundreds of ovaries. Based on detailed gonadal histology (Figure 8A–D), these worms can be divided into two contrasting stages of sexual development. Worms in the effectively female phase had some large oocytes surrounded by a jelly layer (Figure 6A, tandem arrow, and Figure 8A, labeled jl) and were

evidently ready for spawning; in addition, the same individuals had numerous testes, each comprising a thin germinal epithelium surrounding a lumen containing few or no sperm (Figure 8A,B). Conversely, worms in the effectively male phase had only small oocytes but had testes with a thick layer of spermatogenic cells, either with or without a mass of sperm in the lumen (Figure 8C,D) and were evidently preparing to function as males. The data on the reproductive biology, in the aggregate (Figure 8E), strongly suggest that a given individual alternates between mating purely as a male or purely as a female. In the absence of any information on the life history, it is unknown whether a young animal spawns initially as a female or as a male or how many alternations in effective sex occur during the life of a given worm.

Although the geographic distribution of *Yoda demiankoopi* n. sp. in the eastern North Pacific is extensive (Figure 1), the individual worms have always been found widely scattered at any given collection site. Consequently, broadcast spawning does not appear to be an option for effecting fertilization, and the worms presumably depend on pairwise encounters. Puzzlingly, however, specimens of *Yoda demiankoopi* n. sp. were not simultaneous but sequential hermaphrodites, which lower the probability that any given pairwise meeting would match individuals of the opposite effective sex. Thus, sequential hermaphroditism would not appear to offer any improvement over the mating success of a gonochoristic species in which sparsely distributed individuals pair randomly. In contrast, the strategy of simultaneous hermaphroditism, which is not uncommon in deep-sea animals (e.g., Kazanidis et al., 2014), favors fertilization whenever any two individuals meet because both ripe eggs and sperm are available. A better understanding of the population biology and detailed behavior of *Yoda demiankoopi* n. sp. might help resolve this paradox.

ACKNOWLEDGMENTS

We are greatly indebted to the Schmidt Ocean Institute, the crew of *R/V Falkor*, the skilled pilots of ROV *SuBastian*, Chief Scientist Lisa Levin, and the science party of FK210726 for the coordinated efforts that resulted in the data presented here. Thanks also to the Schmidt Ocean Institute for permission to use the live images of *Yoda demiankoopi* n. sp. and for supporting the open access publication of this study. We also thank Linda Khunz, David Clague, and Lonny Lundsten of MBARI for collecting and processing specimens during Dive 176 of the ROV *Doc Ricketts* and for providing us with archived data. MBARI expeditions are supported by the David and Lucile Packard Foundation. Charlotte Seid capably helped access museum specimens from the SIO Benthic Invertebrate Collection. We also thank Marina McCowin for DNA extraction and Sanger sequencing. Our manuscript was improved by the criticisms of Linda Z. Holland. We thank the Editor in Chief, Mike Hart, and reviewers Chris Cameron and Karen Osborn for their helpful comments on the initial submission.

CONFLICT OF INTEREST

The authors have no conflict of interest to declare. GWR is an editor for *Invertebrate Biology* but played no part in the review process.

ORCID

Nicholas D. Holland https://orcid.org/0000-0002-3448-490X
Avery S. Hiley https://orcid.org/0000-0001-8956-5080
Greg W. Rouse https://orcid.org/0000-0001-9036-9263

REFERENCES

Allio, R., Schomaker-Bastos, A., Romiguier, J., Prosdocimi, F., Nabholz, B., & Delsuc, F. (2020). MitoFinder: Efficient automated large-scale extraction of mitogenomic data in target enrichment phylogenomics. *Molecular Ecology Resources*, *20*, 892–905. https://doi.org/10.1111/1755-0998.13160

Bateson, W. (1885). The later stages in the development of *Balanoglossus kowalevskii*, with a suggestion as to the affinities of the Enteropneusta. *Quarterly Review of Microscopical Science*, *25*, 81–122.

Benito, J. (1975). Estudio histoquímico de la epidermis de *Glossobalanus minutus* (Kowalewsky) (Ptychoderidae, Enteropneusta, Hemichordata). *Boletín de la Real Sociedad Española de Historia Natural (Sección Biológica)*, *73*, 229–235.

Benito, J., Fernández, I., & Prados, F. (1993). Fine structure of the hepatic sacculations of *Glossobalanus minutus* (Enteropneusta, Hemichordata). *Acta Zoologica Stockholm*, *74*, 77–86.

Bernt, M., Donath, A., Jühling, F., Externbrink, F., Florentz, C., Fritzsch, G., Pütz, J., Middendorf, M., & Stadler, P. F. (2013). MITOS: Improved de novo metazoan mitochondrial genome annotation. *Molecular Phylogenetics and Evolution*, *69*, 313–319. https://doi.org/10.1016/j.ympev.2012.08.023

Bolger, A. M., Lohse, M., & Usadel, B. (2014). Trimmomatic: A flexible trimmer for Illumina sequence data. *Bioinformatics*, *30*, 2114–2120. https://doi.org/10.1093/bioinformatics/btu170

Cannon, J. T., Kocot, K. M., Waits, D. A., Swalla, B. J., Santos, S. R., & Halanych, K. M. (2014). Phylogenomic resolution of the hemichordate and echinoderm clade. *Current Biology*, *24*, 2827–2832. https://doi.org/10.1016/j.cub.2014.10.016

Cannon, J. T., Rychel, A. L., Eccleston, H., Halanych, K. M., & Swalla, B. J. (2009). Molecular phylogeny of Hemichordata, with updated status of deep-sea enteropneusts. *Molecular Phylogenetics and Evolution*, *52*, 17–24. https://doi.org/10.1016/j.ympev.2009.03.027

Cannon, J. T., Swalla, B. J., & Halanych, K. M. (2013). Hemichordate molecular phylogeny reveals a novel cold-water clade of harrimaniid acorn worms. *Biological Bulletin*, *225*, 194–204. PMID: https://doi:10.1086/BBLv225n3p194

Casselman, W. G. B. (1959). *Histochemical Technique*. Methuen.

Darriba, D., Posada, D., Kozlov, A. M., Stamatakis, A., Morel, B., & Flouri, T. (2020). ModelTest-NG: A new and scalable tool for the selection of DNA and protein evolutionary models. *Molecular Biology and Evolution*, *37*, 291–294. https://doi.org/10.1093/molbev/msz189

Edgar, R. C. (2004). MUSCLE: Multiple sequence alignment with high accuracy and high throughput. *Nucleic Acids Research*, *32*, 1792–1797. https://doi.org/10.1093/nar/gkh340

Edler, D., Klein, J., Antonelli, A., & Silvestro, D. (2021). Raxm1GUI 2.0: a graphical interface and toolkit for phylogenetic analyses using RaxML. *Methods in Ecology and Evolution*, *12*, 373–377. https://doi.org/10.1111/2041-210X.13512

Ezhova, O. V., Lukinyh, A. I., Galkin, S. V., Krylova, E. M., & Gebruk, A. V. (2022). Deep-sea acorn worms (Enteropneusta) from the Bering Sea with a description of a new genus and a new species of Torquaratoridae dominating soft-bottom communities. *Deep Sea Research, Part II: Topical Studies in Oceanography*, *195*, 105014. https://doi.org/10.1016/j.dsr2.2021.105014

Gegenbaur, C. (1870). *Grundzüge der vergleichenden Anatomie; Zweite Auglage*. Engelmann.

Gill, G. W., Frost, J. K., & Miller, K. A. (1974). New formula for a half-oxidized hematoxylin solution that neither overstains nor requires differentiation. *Acta Cytologica*, *18*, 300–311.

Giribet, G., Carranza, S., Baguña, J., Ruitort, M., & Ribera, C. (1996). First molecular evidence for the existence of a Tardigrada + Arthropoda clade. *Molecular Biology and Evolution*, *13*, 76–84. https://doi.org/10.1093/oxfordjournals.molbev.a025573

Halanych, K. M., Cannon, J. T., Mahon, A. R., Swalla, B. J., & Smith, C. R. (2013). Modern Antarctic acorn worms form tubes. *Nature Communications*, *4*, 1–4. https://doi.org/10.1038/ncomms3738/www.nature.som/nature.communications

Hein, J. R., Reid, J. A., Conrad, T. A., Clague, D. A., Schulz, M. S., & Davis, A. S. (2010). *Seamounts and ferromanganese crusts within and near the U.S. EEZ off California. Data for Farnella Cruise F-787-SC*. USGS. Open-File Report 10-1069

Holland, N. D., Clague, D. A., Gordon, D. P., Gebruk, A., Pawson, D. L., & Vecchione, M. (2005). "Lophenteropneust" hypothesis refuted by collection and photos of new deep-sea hemichordates. *Nature*, *434*, 374–376. https://doi.org/10.1038/03382

Holland, N. D., Jones, W. J., Elena, J., Ruhl, H. A., & Smith, K. L. (2009). A new deep-sea species of epibenthic acorn worm (Hemichordata, Enteropneusta). *Zoosystema*, *31*, 333–346. https://doi.org/10.5252/z2009n2a6

Holland, N. D., Khunz, L. A., & Osborn, K. J. (2012). Morphology of a new deep-sea acorn worm (Class Enteropneusta, Phylum Hemichordata): A part-time demersal drifter with externalized ovaries. *Journal of Morphology*, *272*, 661–671. https://doi.org/10.1002/jmor.20013

Humason, G. L. (1962). *Animal Tissue Techniques*. Freeman.

Jabr, N., Archambault, P., & Cameron, C. B. (2018). Biogeography and adaptations of torquaratorid acorn worms (Hemichordata: Enteropneusta) including two new species from the Canadian Arctic. *Canadian Journal of Zoology*, *96*, 1221–1229. https://doi.org/10.1139/cjz-2017-0214

Katoh, K., & Standley, D. M. (2013). MAFFT multiple sequence alignment software version 7: improvements in performance and usability. *Molecular Biology and Evolution*, *30*, 772–780. https://doi.org/10.1093/molbev/mst010

Kazanidis, G., Typer, P. A., & Billet, D. S. M. (2014). On the reproduction of the simultaneous hermaphrodite *Paroriza prouhoi* (Holothuroidea: Synallactidae) in the Porcupine Abyssal Plain, north-east Atlantic. *Journal of the Marine Biological Association of the United Kingdom*, *94*, 847–856. https://doi.org/10.1017/S0025315413001537

Kearse, M., Moir, R., Wilson, A., Stones-Havas, S., Cheung, M., Sturrock, S., Buxton, S., Cooper, A., Markowitz, S., Duran, C., Thierer, T., Ashton, B., Meintjes, P., & Drummond, A. (2012). Geneious Basic: An integrated and extendable desktop software platform for the organization and analysis of sequence data. *Bioinformatics*, *28*, 1647–1649. https://doi.org/10.1093/bioinformatics/bts199

Kozlov, A. M., Darriba, D., Flouri, T., Morel, B., & Stamatakis, A. (2019). RaxML-NG: A fast, scalable and user-friendly tool for maximum likelihood phylogenetic inference. *Bioinformatics*, *35*, 4453–4455. https://doi.org/10.1093/bioinformatics/btz305

Laslett, D., & Canbäck, B. (2008). ARWEN: A program to detect tRNA genes in metazoan mitochondrial nucleotide sequences. *Bioinformatics*, *24*, 172–175. https://doi.org/10.1093/bioinformatics/btm573

Leigh, J. W., & Bryant, D. (2015). POPART: full-feature software for haplotype network construction. *Methods in Ecology and Evolution*, *6*, 1110–1116. https://doi.org/10.1111/2041-210x.12410

Li, Y. N., Kocot, K. M., Tassia, M. G., Cannon, J. T., Bernt, M., & Halanych, K. M. (2019). Mitogenomics reveals a novel genetic code in Hemichordata. *Genome Biology and Evolution*, *11*, 29–40. https://doi.org/10.1093/gbe/evy254

Li, D., Luo, R., Liu, C. M., Leung, C. M., Ting, H. F., Sadakane, K., Yamashita, H., & Lam, T. W. (2016). MEGAHIT v1.0: A fast and scalable metagenome assembler driven by advanced methodologies and community practices. *Methods*, *102*, 3–11. https://doi.org/10.1016/j.ymeth.2016.02.020

Meek, A. (1922). *Glossobalanus marginatus*, a new species of Enteropneusta from the North Sea. *Quarterly Journal of Microscopical Science*, *66*, 579–594.

Osborn, K. J., Gebruk, A. V., Rogacheva, A., & Holland, N. D. (2013). An externally brooding acorn worm (phylum Hemichordata, class Enteropneusta, family Torquaratoridae) from the Russian Arctic. *Biological Bulletin*, *225*, 113–123. PMID: https://www.jstor.org/stable/23595226

Osborn, K. J., Khunz, L. A., Priede, I. G., Urata, M., Gebruk, A. V., & Holland, N. D. (2012). Diversification of acorn worms (Hemichordata, Enteropneusta) revealed in the deep sea. *Proceedings of the Royal Society B*, *279*, 1646–1654. https://doi.org/10.1098/rspb.2011.1916

Palumbi, S. R. (1996). Nucleic acids II: The polymerase chain reaction. In D. M. Hillis, C. Moritz, & B. K. Mable (Eds.), *Molecular Systematics* (2nd ed.) (pp. 205–247). Sinauer.

Pearse, J. S. (1965). Reproductive periodicities in several contrasting populations of *Odontaster alidus* Koehler, a common Antarctic asteroid. *Antarctic Research Series*, *5*, 39–85.

Priede, I. G., Osborn, K. J., Gebruk, A. V., Jones, D., Shale, D., Rogacheva, A., & Holland, N. D. (2012). Observations on torquaratorid acorn worms (Hemichordata, Enteropneusta) from the North Atlantic with descriptions of a new genus and three new species. *Invertebrate Biology*, *131*, 244–257. https://doi.org/10.1111/j.1744-7410.2012.00266x

Romero-Romero, S., Miller, E. C., Black, J. A., Popp, B. N., & Drazen, J. C. (2021). Abyssal deposit feeders are secondary consumers of detritus and rely on nutrition derived from microbial communities in their guts. *Scientific Reports*, *11*, article 12594. https://doi.org/10.10338/s41598-021-91927-4

Spengel, J. W. (1893). *Die Enteropneusten des Golfes von Neapel und der angrenzenden Meeres-Abschnitte*. Monographie 18, Enteropneusten. Friedländer.

Spengel, J. W. (1901). Die Benennung der Enteropneusten-Gattungen. *Zoologische Jahrbücher, Abteilung für Systematik, Geographie und Biologie der Tiere*, *15*, 209–218.

Spicer, S. S. (1963). Histochemical differentiation of mammalian mucopolysaccharides. *Annals of the New York Academy of Sciences*, *106*, 379–388.

Steiner, G. (1994). Variations in the number of intestinal loops in Scaphopoda (Mollusca). *Marine Ecology*, *15*, 165–174.

Whiting, M. F., Carpenter, J. C., Wheeler, Q. D., & Wheeler, W. C. (1997). The Strepsiptera problem: phylogeny of the homometabolous insect orders inferred from *18S* and *28S* ribosomal DNA sequences and morphology. *Systematic Biology*, *46*, 1–68.

Willey, A. (1899). Remarks on some recent work on the Protochorda, with a condensed account of some fresh observations on the Enteropneusta. *Quarterly Review of Microscopical Science*, *42*, 223–244.

Worsaae, K., Sterrer, W., Kaul-Strehlow, S., Hay-Schmidt, A., & Giribet, G. (2012). An anatomical description of a miniaturized acorn worm (Hemichordata, Enteropneusta) with asexual reproduction by paratomy. *PLoS ONE*, *7*, article e48529. https://doi.org/10.1371/journal.pone.0048529

How to cite this article: Holland, N. D., Hiley, A. S., & Rouse, G. W. (2022). A new species of deep-sea torquaratorid enteropneust (Hemichordata): A sequential hermaphrodite with exceptionally wide lips. *Invertebrate Biology*, *141*(3), e12379. https://doi.org/10.1111/ivb.12379